A high-content screening platform utilizing polarization anisotropy and FLIM microscopy

Daniel. R. Matthews[a], Simon M. Ameer-Beg[b], Paul Barber[c], Glenn P. Pierce[c], Robert G. Newman[c], Boris Vojnovic[c], Leo M. Carlin[b], Melanie D. Keppler[b], Tony Ng[b], Klaus Suhling[d], Malcolm Irving[a]
[a]Randall Division, King's College London, New Hunt's House, Guy's Medical School Campus, London, SE1 1UL.
[b]Dimbleby Department of Cancer Studies, King's College London, New Hunt's House, Guy's Medical School Campus, London, SE1 1UL.
[c]Advanced Technology Division, University of Oxford, Gray Cancer Institute, PO Box 100, Mount Vernon Hospital, Northwood, Middlesex, HA6 2JR.
[d]Department of Physics, King's College London, Strand, London, WC2R 2LS.

ABSTRACT

An automated high-content screening microscope has been developed which uses fluorescence anisotropy imaging and fluorescence lifetime microscopy to identify Förster resonant energy transfer between eGFP and mRPF1 in drug screening assays. A wide-field polarization resolved imager is used to simultaneously capture the parallel and perpendicular components of both eGFP and mRFP1 fluorescence emission to provide a high-speed measurement of acceptor depolarization. Donor excited state lifetime measurements performed using laser scanning microscopy is then used to determine the FRET efficiency in a particular assay. A proof-of-principle assay is performed using mutant Jurkat human T-cells to illustrate the process by which FRET is first identified and then quantified by our high-content screening system.

Keywords: High-content screening, fluorescence anisotropy, FLIM, FRET

1. INTRODUCTION

Recently there has been a paradigm shift in the exploration of drug compounds for cancer therapeutics; a shift from screening at the genomic to the proteomic level. The large-scale gene sequencing programs of the last few decades are providing valuable information in the area of drug discovery but recently there has been a directed effort to find targets and leads by means of the gene products rather than the genes themselves. In essence this approach is one where protein interactions or post-translational modification events (such as phosphorylation, or ubiquitinylation) are monitored at the level of the entire genome. This, almost systems biology, philosophy has arisen due to the realization that monitoring disease function at the level of individual genes is too simplistic; it is the perturbation of gene products, combinations and interactions of several proteins, that make up the field of proteomics, that can provide the means by which drug discovery can most efficiently occur. Given that predications for the number of proteins are at the level of 30,000 and the number of permutations for possible interactions to be monitored increases this number by a factor of ten, it is clear that a high-throughput approach to proteomics, where spatial and temporal information content is not compromised by the speed-optimized assays, is essential[1].

The importance of fluorescence microscopy to the life sciences cannot be underestimated: it has proven an essential tool in any number of different fields and high-throughput/content screening is no exception. Screening at the cellular and even sub-cellular level by fluorescence microscopy provides a number of technological challenges but ultimately the information yielded by monitoring interactions in the cellular environment outweigh these challenges. Viewing protein interactions, perturbations and post-translational modifications within a biologically relevant environment to produce unambiguous information has lead to the development of a number of technologies for automated high-throughput microscopy where everything from sample preparation, image acquisition and analysis is performed unsupervised to free-up the user for more important tasks. In fact a number of wide-field (e.g. "Scan^R" from Olympus), and even confocal, (e.g. "IN Cell Analyzer 3000" from GE Healthcare) systems are now commercially

available which include multi-channel detection, automated focus identification and software for image acquisition and data analysis. However, these systems are basically all based on measuring fluorescence intensity and screening is done on the basis of phenotypic alteration under the action of a drug or pathogen.

The control of cellular function and intracellular signalling is clearly complex and highly regulated. Many signalling cascades have been extensively investigated and the relationships between proteins have been partially delineated using biochemical techniques. Microscopical techniques coupled with immuno-cytochemical methods allow us to preserve and image the relative localisation of multiple signalling molecules in cellular compartments under quiescent or stimulated conditions. Whilst a degree of localisation of proteins is conferred using these techniques, the spatial resolution afforded by conventional, far-field microscopy is insufficient to resolve the specific inter-relationship between individual protein complexes occurring on the nanometer length scale. Measurement of the near-field localisation of protein complexes may be achieved by the detection of Förster resonance energy transfer (FRET) between protein-conjugated fluorophores[2]. FRET is a non-radiative, dipole-dipole coupling process whereby energy from an excited donor fluorophore is transferred to an acceptor fluorophore in close proximity[3, 4]. The dependence of the coupling efficiency varies with the inverse sixth power of the distance between acceptor and donor and is typically described in terms of the Förster radius (distance at which the efficiency of energy transfer is 50%), typically of the order 1-10 nm. Excitation of the donor sensitises emission from the acceptor that ordinarily would not occur. Since the process depletes the excited state population of the donor, FRET will both reduce the fluorescence intensity and the donor fluorescence lifetime. The advantage of using donor fluorescence lifetime microscopy (FLIM) to detect FRET is that the method is independent of fluorophore concentration, donor-acceptor stochiometry and light path length and is therefore well suited to studies in intact cells[5-9]. Combined with confocal or multiphoton microscopical techniques to examine the localisation of effects in cellular compartments, FLIM/FRET techniques allow us to determine populations of interacting protein species on a point-by-point basis at each resolved voxel in the cell[10-15]. Whilst FLIM remains the gold standard for measurement of FRET, particularly when we consider issues such as interacting/non-interacting fractions of donors, there is a need for faster metrics when dealing with dynamic events or when measurement time must be minimised. For high-content screening the typical measurement time for appropriate

In this paper we discuss the development of an in-house high-content screening system which incorporates wide-field fluorescence anisotropy microscopy and fluorescence lifetime microscopy on a single automated system to screen proteomic interactions. The assays to be screened are all based upon FRET between green and red fluorescent proteins. Briefly the assays performed here are broadly of two types. In the first, the assay is based on Riachu biosensors[16] comprising eGFP and mRFP1 separated by active sensing protein sub-units such that upon activation the biosensor changes conformation bring the fluorescent proteins in close proximity thereby increasing the FRET efficiency. We have recently established novel biological tools for imaging Rho GTPase activities in cells, by employing high-resolution, multiphoton FLIM[10, 17]. Raichu probes (for Cdc42, Rac1 and RhoA) were constructed in our laboratory, on the basis of the original design by Matsuda and co-workers. Raichu-Rac and Raichu-Cdc42 use Rac and Cdc42 as the sensor regions and the CRIB region of Pak as the ligand region. For Raichu-RhoA, the Rho-bind domain of Rhotekin is the ligand region. The new constructs allow us to obtain FLIM images of GTPase activity for monitoring FRET between GFP[18] and a monomeric Red Fluorescent Protein (mRFP1)[19]. On conversion from GDP- to GTP-bound state, Rac1/Cdc42 binds to Pak, enabling the energy transfer from GFP (donor) to mRFP1 (acceptor) and shortening GFP fluorescence lifetime. The use of such biosensor probes for HCS applications is appealing, since there is 1:1 stochiometry between donors and acceptors, making the analysis of data more straightforward. For the second, more challenging, application; protein-protein interaction between protein heterodimers labeled either with eGFP or mRFP1 may be considered. Depending on the purpose of the screen, the protein pair can be chosen such that an external event (such as drug addition) causes a gain or loss of association between proteins such that eGFP and mRFP1 are close enough to exchange energy non-radiatively. Such a protein-protein hetero-FRET experiment is more complex in this context because, protein stochiometry is hard to control and in some circumstances a non-interacting pool of proteins may exist, swamping the specific interaction.

The system described here is based on two levels of screening of the FRET interaction between the fluorescent proteins. Wide-field fluorescence anisotropy microscopy is used in a first-pass to determine possible hits in the assay where biosensor activity is perturbed from the mean control behaviour (note that this activity can either increase or decrease since we are measuring Rho-GTPase activity which in quiescent cells is non-zero). The second pass uses the laser scanning component of the instrument to provide a detailed FLIM analysis of the identified hits in order to fully quantify the level of interaction, knockdown or activation taking place, depending on the particular assay. In this way we combine a high-speed, high-throughput methodology with more rigorous, information driven, measurements. In the

remainder of the paper section 2 provides details of the hardware and microscope construction. A description of the fluorescence anisotropy component of the system and its use in identifying FRET is given in section 3, and section 4 presents details of an example assay where FRET has been identified by anisotropy measurements and the efficiency is determined by FRET-FLIM.

2. INSTRUMENTATION

The HSC instrument is broadly based on an inverted microscope but here every component is selected with automation in mind. There are a number of high-throughput and high-content systems currently on the market but here we have taken the approach of developing an in-house system since these commercially available systems are generally speaking not flexible and would not allow any user modifications. Many of these systems are based around intensity measurements and currently there has been just a single example reported of a high throughput system with incorporates a fluorescence lifetime element, which in this case was based on frequency domain measurements[20].

In the high-content screening microscope reported here the user can select between wide-field and laser scanning excitation for both intensity and time-domain measurements. In wide-field mode the output from a fibre coupled mercury lamp (Nikon Intensilight) is de-magnified and focussed onto the pupil of the 20x plan fluor objective lens after first being linearly polarized. As discussed earlier, the wide-field mode of the instrument is used to capture anisotropy information from the sample and the necessary linear polarized excitation is achieved by means of two appropriately placed polarizing beam-splitters and a half-wave to rotate the plane of the polarized excitation such that it is parallel or perpendicular to the plane of emission polarizers. In this scheme the fluorescence emission from the sample of interest is detected by a polarization-resolved imager (Optical Insights Quadview Image Splitter) that separates the emission according to both wavelength and polarization. A single CCD (Hamamatsu Orca) image therefore provides four spatially identical images that differ in their wavelength and polarization content. The screens of interest for this system are interactions between green and red fluorescent proteins (eGFP and mRFP1 respectively) and as such the polarization resolved imager captures two orthogonal polarizations at wavelengths of 515±30 nm and 630±70 nm (filters provided by Chroma Technologies).

The laser-scanning element of the microscope has been incorporated to allow the user to perform FLIM-FRET assays or screens. The excitation is provided by a white-light supercontinuum laser (SC450-4, Fianium) that emits 4 ps pulses at a repetition rate of 40 MHz with an average power of 4W in a wavelength range of 470-2000 nm (2mW/nm). This enormous wavelength range makes the instrument extremely versatile and allows us to excite both the donor and acceptor in any number of FLIM-FRET assays. At present we are interested in observing an interaction in the eGFP-mRFP1 pairing in a number of scenarios (to be discussed below) and as such we filter the laser output with a 488±10 nm bandpass filter to excite the eGFP component only.

The collimated output from the fibre of the laser has a nominal beam-waist of 3.3 mm, a diameter too small to adequately fill the pupil of our objective, and as such we expand the beam using a 1:2 achromatic telescope post spectral filtering. The beam is directed into an in-house designed afocal scanning component which uses two mirrors to provide bi-directional scanning of the focal plane of the objective lens. The afocal system is used to produce a stationary pupil plane. Detection of fluorescence emission is achieved by non-descanned detection using a photomultiplier tube (PMT-100, Hamamatsu), the output of which is routed to a SPC-830 time-correlated single photon counting personal computer plug-in board (Becker and Hickl).

The instrument is equipped with a motorized stage (Märzhauser), a closed-loop objective focusing mount (Piezo-Jena Mipos) with a 500 μm range of travel, a motorized filter cube selector and a motorized component allowing selection of either wide-field of laser scanning excitation. All of these components are controlled using USB communication, via the I^2C protocol, and with an integrated modular software package developed at the Gray Cancer Institute by P. Barber and G. Pierce. The software provides the user with the ability to control every aspect of image acquisition including access to the Python scripting language for complete automation of an assay or screen. Currently image processing is performed off-line using ImageJ and Matlab but this will eventually be incorporated into an integrated package since we envisage the screens and assays taking place in two distinct stages. The first, anisotropy based, level of the screen will be used to identify potential hits and as such will individually interrogate each well in a multi-well plate and therefore the anisotropy will be calculated on-line before the second, lifetime-based, stage can

proceed. It is less critical for the FLIM data to processed online since there will potentially be less images for the user to process since the only the hit-wells will be analyzed.

3. FLUORESCENCE ANISOTROPY MICROSCOPY

The concept of fluorescence polarization (or anisotropy) microscopy has proven to be highly capable of identifying changes of the microenvironment of fluorescent molecules such as orientation and viscosity. At present the technique has been employed in dynamic measurements, where the rotational correlation time of a molecule is determined, in either the time[21, 22] or frequency domain[23], both have which have been utilized in wide-field microscopy.

Steady-state fluorescence anisotropy has been shown to be a powerful technique for measurement of FRET for both protein homodimers[24] (where FLIM alone cannot resolve interaction) and, more recently, heterodimers[25, 26]. In each case, the measurement principle differs in the sign of the change in anisotropy. For homo-FRET, the observed anisotropy of the donor is reduced since energy is incoherently exchanged between spectrally similar fluorophores. For hetero-FRET, the donor anisotropy is observed to increase slightly (due to its dependence on the fluorescence lifetime in the Perrin equation (equation (1)) whilst the anisotropy of the acceptor is dramatically reduced due to breaking of photoselection due to energy transfer.

$$\frac{1}{r} = \frac{1}{r_0} + \frac{\tau}{r_0 \theta} \tag{1}$$

This effect is significant only when the rotational correlation time of the probes is slow with respect to the rate of transfer. The process is analogous to sensitised emission FRET, however, the measurement of anisotropy reduces some requirement for correction since both bleed though of donor into acceptor channel and non-resonant excitation of acceptors will increase the anisotropy and therefore introduce an underestimate of anisotropy for the interacting fraction. In fact, this effect has been used to some advantage by Mattheyses et al.[25] to determine the interacting population in a protein-protein interaction without intrinsic 1:1 donor:acceptor stochiometry.

Steady-state anisotropy is determined by measuring the intensity parallel and perpendicular to the orientation of the excitation photons as shown in equation (2):

$$r = \frac{I_{vv} - GI_{vh}}{I_{vv} + 2GI_{vh}} \tag{2}$$

Here r is the steady state anisotropy, Ivv and Ivh are the fluorescence emission intensities measured parallel and perpendicular respectively for the case where the linear polarization of the excitation is oriented vertically. The factor G is used to account for the different efficiencies for measurement of parallel and perpendicular polarizations within the system. In a microscope, where the excitation and detection paths are essentially collinear the necessary correction is:

$$G = \sqrt{\frac{I_{vv} I_{hv}}{I_{hh} I_{vh}}} \tag{3}$$

A number of other factors must be considered. The efficiencies of the detection polarizers are extremely important for obtaining the anisotropy. In our polarization resolved imager we find a high efficiency in the green channel, but in the red channel there is a bleed through of the orthogonal polarization in each window of the order of

10%. Following Siegel et. al.[22], who also encounter this problem in their wide-field time-resolved anisotropy system, we correct this bleed-through as follows:

$$I_{vvcorr} = \frac{9I_{vvmeasured} - I_{vhmeasured}}{8} \tag{4}$$

$$I_{vhcorr} = \frac{9I_{vhmeasured} - I_{vvmeasured}}{8} \tag{5}$$

In addition to this polarization bleed through it is also necessary to correct for any background counts and spectral bleed-through of excitation light in the green channel and eGFP emission appearing in the mRFP1 channel all of which cause the anisotropy to be underestimated. There is also one other correction that needs to be applied that is peculiar to this polarization resolved imaging system. We find that each detection channel is slightly rotated with respect to the other windows due to the mechanical tolerances involved in positioning each of the optical components, meaning that they do not spatially overlap. The figure below shows a "raw" image of a "green" fluorescent block whose emission spectrum is broad enough for photons to be detected in both channels of the imager. This image, where the colored boxes are a guide-for-the-eye, illustrates the degree of rotation required if pixel colocalization is to be achieved.

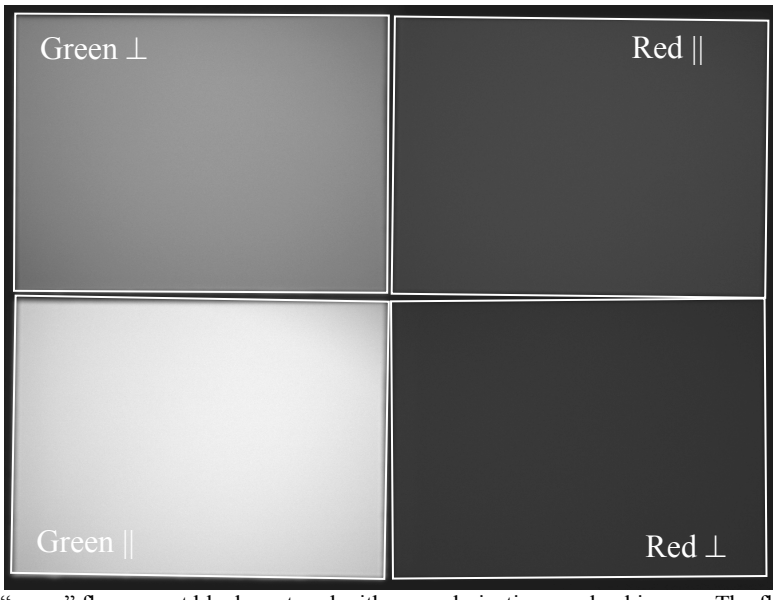

Fig. 1. An image of a "green" fluorescent block captured with our polarization resolved imager. The fluorescence has a broad enough bandwidth that emission is detected in both green and red channels. This image demonstrates the degree of rotation in each of the "windows" of the imager which must be corrected in order to perform anisotropy measurements.

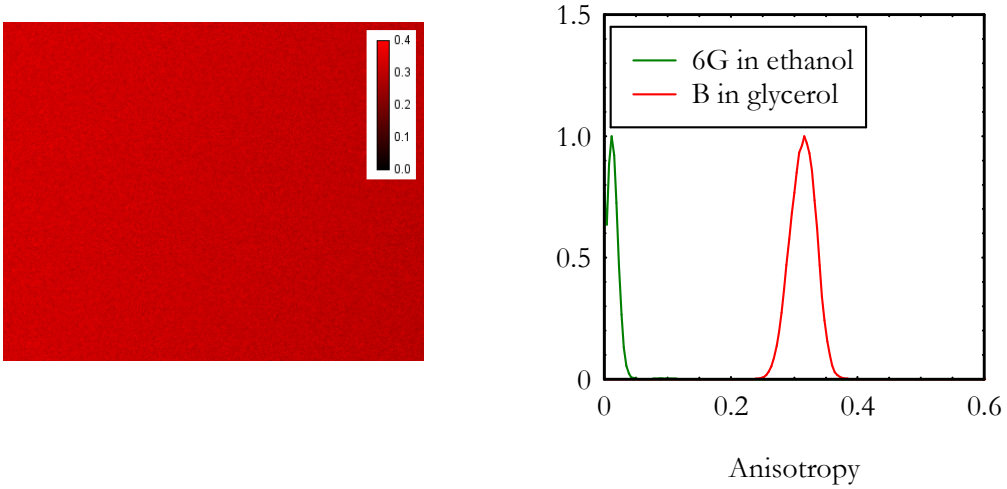

Fig. 2. (a) An anisotropy image of a solution of Rhodamine B dissolved in glycerol; and (b) a comparison with a solution of Rhodamine 6G dissolved in methanol plotted in the form of histogram of anisotropy as a function of number of pixels (subsequently normalised).

When the necessary corrections have been performed the system is capable of producing anisotropy images as figure 2 illustrates. In 2(a) we show an anisotropy image of a solution of Rhodamine B that has been dissolved in glycerol, derived from the red channel of microscope. The plot of anisotropy as a function of number of pixels in 2(a) shows that there is very little rotational depolarization of the Rhodamine B molecules when dissolved in Glycerol resulting in a high anisotropy value of 0.32. As a comparison we also imaged a Rhodamine 6G solution in methanol (captured by the green channel of the microscope) that showed, due to its relatively fast rotational correlation time, a steady-state anisotropy of 0.08. The values of anisotropy obtained while changing the solvent viscosity is typical for these small molecules, and the width of the histograms demonstrates that there was very little variation across the images as expected when the various corrections are applied and the G-factor is accounted for.

4. FRET IDENTIFICATION

4.1 Acceptor FRET measured by Anisotropy

Identification of FRET in polarization microscopy works best when the FRET pairs are highly rigid molecules, in the sense that their rotational correlation time is much greater than their excited state lifetime. It turns out that fluorescent proteins (FPs) are just such molecules. For example it has been shown that the anisotropy of eGFP in solution is of the order of 0.3 (of course this value can change with variation of a number of factors such as solvent viscosity and concentration) since it has slow rotational correlation time in the region of 15-20 ns, as compared to its excited state lifetime which is typically of the order of 2.2 ns. It is well known that energy transfer can be a mechanism for depolarization and under conditions where FRET occurs between a pair of FPs the highly polarized nature of the donor and the unconstrained orientation of the acceptor molecule means that the non-radiative transfer of energy can result in a strong depolarization of the acceptor molecule. The sensitized emission can therefore display a low value of anisotropy compared to the donor, and indeed a non-interacting acceptor molecule. Large changes of anisotropy can occur for the sensitized emission for modest values of FRET efficiency resulting in an extremely sensitive, high dynamic range, measurement of the interaction between the FRET pair. In a high-content screen any drug, RNAi or inhibitor, or the interaction of the FPs can therefore be identified in a straight-forward and rapid manner using fluorescence polarization microscopy.

4.2 Identification of FRET in T-cells

To test the performance of our system we examine the activation of an eGFP/mRFP1 variant of the Raichu-cdc42 biosensor in a mutant of the Jurkat human T-cell line. The drug screens of interest to be performed on the fully automated system will examine a variety of cancer cell lines but here we have chosen to use a β_1 integrin assay in T-cells. The properties of the biosensor in this system have been well characterized in our lab and show little heterogeneity, with high FRET efficiency upon activation therefore serving to amply demonstrate the capability of our system. Currently we are developing cancer cell line assays for use with high-content system including a screen of a library of 200 compounds which will be reported in a separate publication. These screens use a similar biosensor system to detect FRET and so the T-cell assays form a good proof-of-principle measurement.

In this assay the control is the A1 version of the T-cells which is a mutant that lacks surface β_1 integrin expression and the control cells are the A1wtβ_1 variation of the same mutant which express wild-type β_1 integrin[27]. The cells were transfected with an the eGFP/mRFP1 variant of the Raichu-Cdc42 FRET probe which results in equal stoichometry of the fluorescent proteins since both are tethered to the biosensor. The Raichu-Cdc42 biosensor is activated when GTP binds Cdc42 which changes the biosensor conformation resulting in an increase in the FRET efficiency[28]. These cells were allowed to settle for 30 minutes at 37°C, 5% CO_2 on glass coverslips coated with 12g10, an activating monoclonal antibody against β_1 integrin. Samples were fixed with Cytofix/Cytoperm (BD) and mounted in Mowiol (Calbiochem) containing 1,4-Diazabicyclo-octane (DABCO; Sigma). Under activation of the β_1 integrin down-stream signaling activates cdc42 resulting in an increased FRET efficiency.

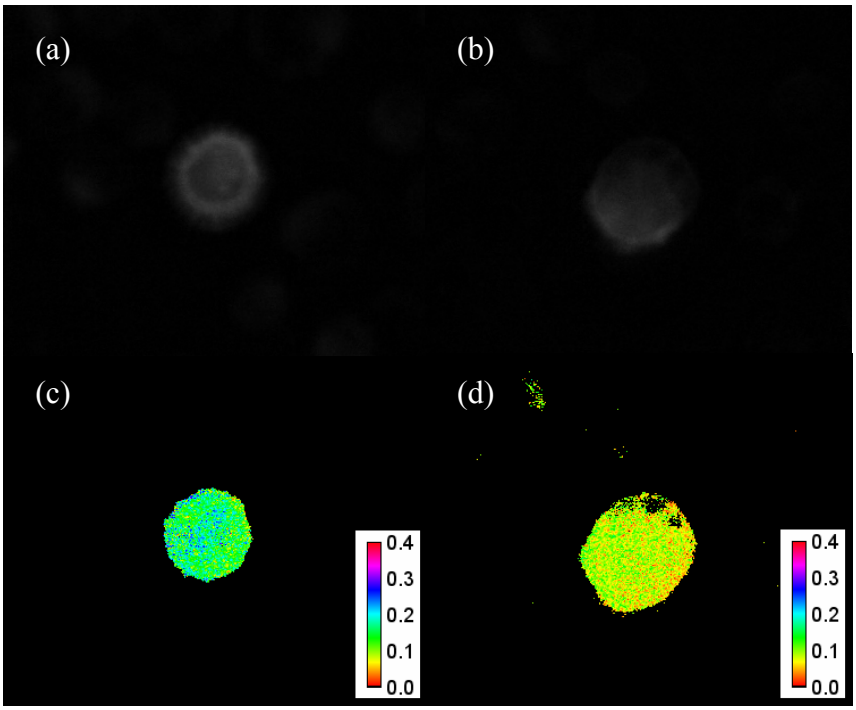

Fig. 3. Images of A1 and A1wtβ_1 mutant T-cells captured in the red channel of the polarization resolved imager. (a) and (b) intensity images of A1 and A1wtβ_1 cells respectively. (c) and (d) anisotropy images of the same cells. The redder colors of the image in (d) indicate an increased FRET efficiency of the A1wtβ_1 cell.

Figure 3 above demonstrates how anisotropy microscopy can be used to identify FRET. Figure 3 (a) and (b) show representative intensity images for A1 and A1wtβ1 cells that will be referred to as control and treated T-cells respectively. These were images using a 40x oil plan fluor objective lens and the polarization resolved imager as described earlier with an exposure time of 1s. It is clear that the cell phenotype is not altered but it is evident that the treated cell is more extended indicating an interaction with the surface bound antibodies. The anisotropy images in figure

3 (c) and (d) show that the steady-state anisotropy is low in both cases indicative of a baseline FRET interaction occurring even in the mutant cells which do not express the β_1 integrin. It is clear that either there is some other down-stream activation of the biosensor, or that its conformation is such that there is already significant energy transfer between the eGFP and mRFP1. However, as the redder color of the cell on this look-up-table illustrates, it is clear that the anisotropy is much lower for the control cell. The graph in figure 4 quantifies the level of difference in anisotropy detected. Here a region of interest is formed around the cell and the anisotropy is plotted as a function of number of pixels (which is subsequently normalized). Although the histograms have a fairly high standard deviation (σ=0.28 for the control and σ=0.29 for the treated cell), due to low signal-to-noise, the difference between the control and treated cells is clear: the anisotropy peaks at 0.13 for the control, and drops to 0.08 for the treated cell indicating an increase in the FRET efficiency.

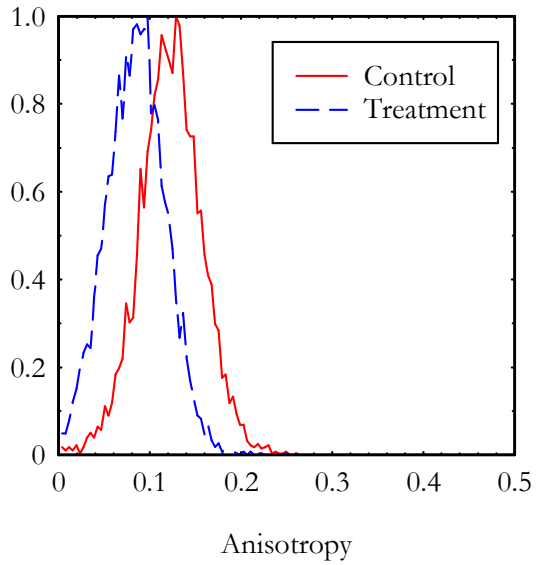

Fig. 4. Histograms generated from the images in Fig. 5. The red curve shows the anisotropy of the A1 cell plotted as a function of the number of pixels (normalized). The low value of anisotropy indicates a baseline activation of the Raichu-cdc42 biosensor resulting in FRET and the depolarization of the mRFP1. The blue curve illustrates the increased FRET efficiency in the A1wtβ_1 cell caused by down-stream activation of cdc42.

4.3 Donor FRET measured by FLIM

Examples of FLIM imaging of the donor eGFP in the T-cells by TCSPC is shown in figure 5. Again intensity images are shown in figure 5 (a) and (b) for a control and treated cell respectively illustrating the much more extended nature of the treated cell indicating a strong interaction with the substrate. Fluorescence lifetime images are constructed by fitting a monoexponential function to each pixel in the image using the TRI2 software written by P. Barber at the Gray Cancer Institute, Oxford University UK. The quality of the fit is judged using the standard χ^2 parameter which in this case is minimized using the Levenberg-Marquadt algorithm. The data analysis proceeds by masking the cell of interest, thresholding the intensity level for pixels to be fitted and then estimating the fit for a small group of pixels. The software is then able to fit to every pixel to generate the FLIM image as shown in figure 5 (c) and (d). It is clear that the eGFP excited state lifetime is much shorter in the treated cell compared to the control being of the order of 1.65 ns and 1.9 ns respectively. Measurement of a biosensor tagged with eGFP only displays a lifetime of the order of 2.2 ns, and when this value is assumed for all pixels in each of the FLIM images the FRET efficiency can be calculated as shown in figure 5 (e) and (f). An examination of a histogram for each of these images, as plotted in figure 6, shows that the FRET efficiency in the control cell is of the order of 15%, increasing to 25% for the treated cell indicating a further activation of the biosensor.

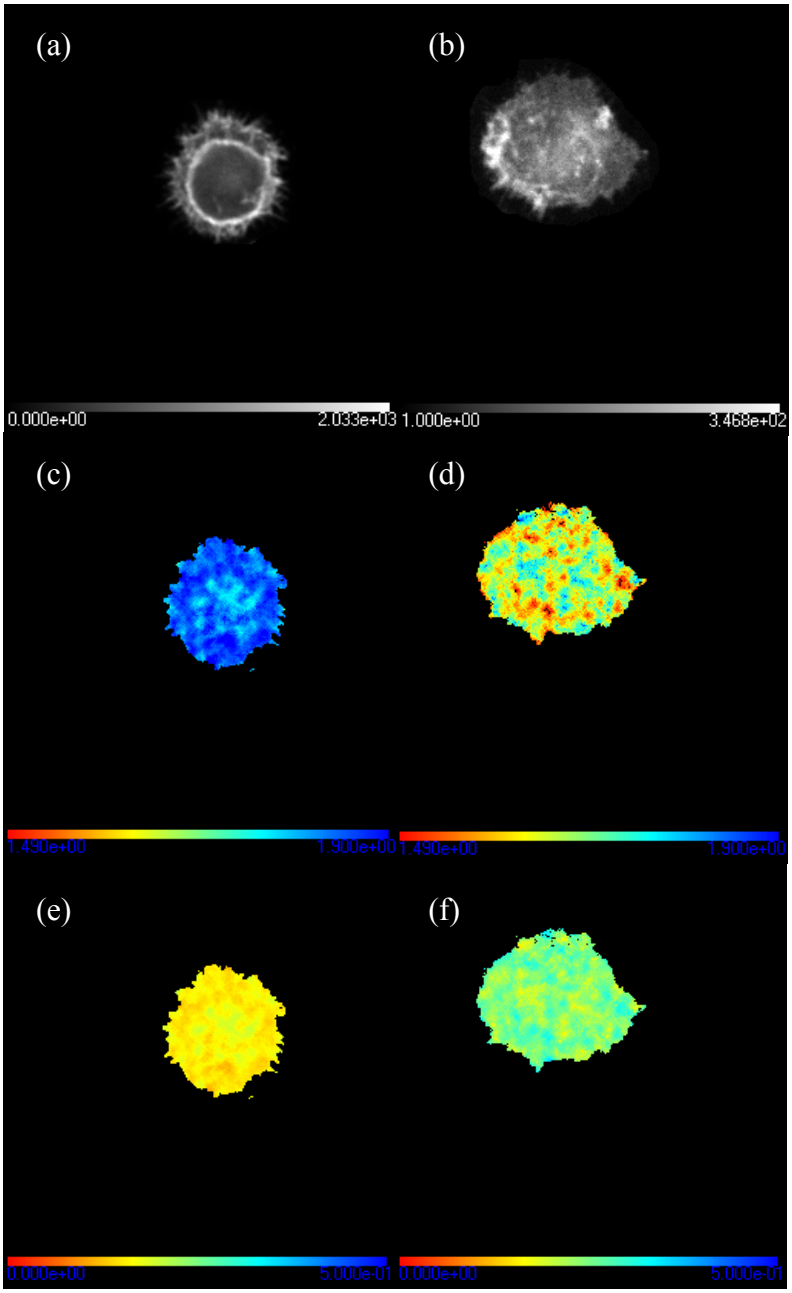

Fig. 5 (a) and (b) intensity images of A1 and A1wtβ_1 cells respectively. (c) and (d) FLIM images of the same cells where the color-bar (same scale in each image) represents the monoexpontential fit to the data. It is clear that the eGFP lifetime is much shorter for the A1wtβ_1 cell expressing the β_1 integrin as compared to the A1 cell. Assuming a non-interacting lifetime of 2.2ns for eGFP leads to the estimations of the FRET efficiency in (e) and (f). Here an efficiency of 15% is measured for the A1 cell which rises to 25% upon activation of cdc42 in the A1wtβ_1 cell.

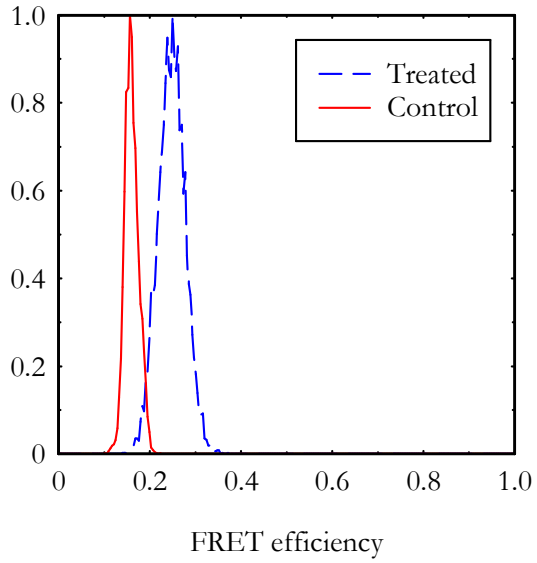

Fig. 6. Histograms derived from the FRET efficiency images in fig. 5. (e) and (f). The data is in good agreement with the anisotropy data presented earlier which suggested an increased FRET efficiency in the A1wtβ_1 cell.

5. DISCUSSION

The T-cell assay described here serves to illustrate the power of combining fluorescence anisotropy imaging with FLIM microscopy. The anisotropy images, captured with the wide-field component of our high-content screening microscope, gave a quick and easy method of determining the presence of an altered FRET efficiency. The images were captured with exposure times of 1s and by employing a macro in ImageJ and some array manipulation in Matlab to split the polarization resolved image into the relevant color and polarization channels, rotate them accordingly and calculate the necessary corrections, a series of anisotropy images could be obtained within a minute or two. The automated component of the microscope was not employed in these proof-of-principle measurements but it is possible to estimate the length of time required to fully automate a 384 well-plate to perform a similar assay with a cancer cell line. Obviously there will be a certain amount of heterogeneity in the assays and therefore it will be necessary to capture at least four regions of interest per well, and for a modest exposure time of 1s this will take a total time of 26 minutes. Taking into account the travel time of the microscope stage and the automated focusing procedure, which initially is software based, would at least double this time. Therefore it should be possible to examine an entire 384 well plate and estimate the FRET efficiency in each well, thereby performing the first level of a screen, in 1-2 hours.

6. SUMMARY

In this paper we have described the development of a high-content screening microscope where everything from the optical layout to the control electronics has been designed and built in-house. The system combines fluorescence anisotropy microscopy, where the depolarization of the acceptor fluorescent proteins in a FRET assay are examined using a polarization resolved imager, with information rich FLIM microscopy where the level of interaction present in an assay is determined by measurement of the donor excited state lifetime. The test assay presented here based on the interaction of T-cells with an monoclonal antibody for β1 integrin elucidated by the presence of the Raichu-cdc42 biosensor, illustrates that anisotropy can be used to give a reliable estimate of the FRET efficiency by observing the resultant depolarization of fluorescence emission of the mRFP1 attached to the biosensor. FLIM microscopy was in good agreement with the wide-field anisotropy imaging showing that this approach can be a powerful tool in high-content screening for drug discovery.

REFERENCES

1 Starkuviene, V. and R. Pepperkok, "The potential of high-content high-throughput microscopy in drug discovery". Br J Pharmacol. **152**(1): p. 62-71.(2007).

2 Jares-Erijman, E.A. and T.M. Jovin, "FRET imaging". Nat Biotechnol. **21**(11): p. 1387-95.(2003).

3 Förster, T., "Intermolecular energy migration and fluorescence". Ann. Physik.**2**: p. 55.(1948).

4 Stryer, L., "Fluorescence Energy Transfer as a spectroscopic ruler". Ann. Rev. Biochem.**47**: p. 819-846.(1978).

5 Ng, T., et al., "Imaging protein kinase Cα activation in cells". Science **283**(5410): p. 2085-9.(1999).

6 Ng, T., et al., "PKCα regulates β1 integrin-dependent cell motility through association and control of integrin traffic". Embo J.**18**(14): p. 3909-23.(1999).

7 Wouters, F.S. and P.I. Bastiaens, "Fluorescence lifetime imaging of receptor tyrosine kinase activity in cells". Curr Biol.**9**(19): p. 1127-30.(1999).

8 Wouters, F.S., P.J. Verveer, and P.I. Bastiaens, "Imaging biochemistry inside cells". Trends Cell Biol.**11**(5): p. 203-11.(2001).

9 Pelet, S., M.J.R. Previte, and P. So, "Comparing the quantification of Förster resonance energy transfer measurement accuracies based on intensity, spectral, and lifetime imaging". J. Biomed. Opt. **11**(3): p. 034017.(2006).

10 Parsons, M., et al., "Spatially distinct binding of Cdc42 to PAK1 and N-WASP in breast carcinoma cells". Mol Cell Biol.**25**(5): p. 1680-95.(2005).

11 Peter, M. and S.M. Ameer-Beg, "Imaging molecular interactions by multiphoton FLIM". Biol Cell.**96**(3): p. 231-6.(2004).

12 Peter, M., et al., "Multiphoton-FLIM quantification of the EGFP-mRFP1 FRET pair for localization of membrane receptor-kinase interactions". Biophys J.**88**(2): p. 1224-37.(2005).

13 Schonle, A., M. Glatz, and S.W. Hell, "Four-dimensional multiphoton microscopy with time-correlated single-photon counting". Appl. Optics. **39**(34): p. 6306-6311.(2000).

14 Duncan, R.R., et al., "Multi-dimensional time-correlated single photon counting (TCSPC) fluorescence lifetime imaging microscopy (FLIM) to detect FRET in cells". J. Microscopy.**215**: p. 1-12.(2004).

15 Calleja, V., et al., "Monitoring conformational changes of proteins in cells by fluorescence lifetime imaging microscopy". Biochem J.**372**(Pt 1): p. 33-40.(2003).

16 Nakamura, T., K. Aoki, and M. Matsuda, "Monitoring spatio-temporal regulation of Ras and Rho GTPase with GFP-based FRET probes". Methods.**37**(2): p. 146-53.(2005).

17 Barber, P.R., et al., "Global analysis of multiphoton time-domain FLIM: Theory and application to protein-protein interactions". in revision for Biophys. J. (2007).

18 Tsien, R.Y., "The green fluorescent protein." Annual Review Biochemistry.**67**: p. 509-544.(1998).

19 Campbell, R.E., et al., "A monomeric red fluorescent protein". Proc Natl Acad Sci U S A. **99**(12): p. 7877-82.(2002).

20 Esposito, A., et al., "Innovating lifetime microscopy: a compact and simple tool for life sciences, screening, and diagnostics". J Biomed Opt.**11**(3): p. 34016.(2006).

21 Suhling, K., et al., "Time-resolved fluorescence anisotropy imaging applied to live cells". Opt Lett. **29**(6): p. 584-6.(2004).

22 Siegel, J., Suhling K., Leveque-Fort S., Webb S. D. Davis D. M., Phillips D., Sabharwal Y., French P. M. W., "Wide-Field time-resolved fluorescence anisotropy imaging (TR-FAIM): Imaging the rotational mobility of a fluorophore". Review of Scientific Instruments. **74**(1): p. 11.(2003).

23 Clayton, A.H., et al., "Dynamic fluorescence anisotropy imaging microscopy in the frequency domain (rFLIM)". Biophys J. **83**(3): p. 1631-49.(2002).

24 Gautier, I., et al., "Homo-FRET microscopy in living cells to measure monomer-dimer transition of GFP-tagged proteins". Biophys J. **80**(6): p. 3000-8.(2001).

25 Mattheyses, A.L., A.D. Hoppe, and D. Axelrod, "Polarized fluorescence resonance energy transfer microscopy". Biophys J. **87**(4): p. 2787-97.(2004).

[26] Rizzo, M.A. and D.W. Piston, "High-contrast imaging of fluorescent protein FRET by fluorescence polarization microscopy″. Biophys J.**88**(2): p. L14-6.(2005).

[27] Romzek, N.C., et al., "Use of a beta1 integrin-deficient human T cell to identify beta1 integrin cytoplasmic domain sequences critical for integrin function″. Mol Biol Cell.**9**(10): p. 2715-27.(1998).

[28] Itoh, R.E., et al., "A FRET-based probe for epidermal growth factor receptor bound non-covalently to a pair of synthetic amphipathic helixes″. Exp Cell Res.**307**(1): p. 142-52.(2005).